Anisotropy effects in a mixed quantum-classical Heisenberg model in two dimensions

1998 J. Phys.: Condens. Matter 10 2065

(http://iopscience.iop.org/0953-8984/10/9/012)

J. Phys.: Condens. Matter **10** (1998) 2065–2079. Printed in the UK PII: S0953-8984(98)85625-7

Anisotropy effects in a mixed quantum–classical Heisenberg model in two dimensions

C Meyers†, Y Meurdesoif†, Y Leroyer† and O Kahn‡

† Centre de Physique Théorique et de Modélisation de Bordeaux, Université Bordeaux I, CNRS, Unité Associée 1537, 19 rue du Solarium, 33174 Gradignan Cédex, France

‡ Laboratoire des Sciences Moléculaires, Institut de Chimie de la Matière Condensée de Bordeaux, CNRS, UPR 9048, Avenue Albert Schweitzer, 33608 Pessac Cédex, France

Received 1 January 1997, in final form 7 October 1997

Abstract. We analyse a specific two-dimensional mixed-spin Heisenberg model with exchange anisotropy, by means of high-temperature expansions and Monte Carlo simulations. The goal is to describe the magnetic properties of the compound $(NBu_4)_2Mn_2[Cu(opba)]_3{\cdot}6DMSO{\cdot}H_2O$ which exhibits a ferromagnetic transition at $T_c = 15$ K. Extrapolating our analysis on the basis of renormalization group arguments, we find that this transition may result from a very-weak-anisotropy effect.

1. Introduction

In the last few years there has been increasing interest in magnetic systems of low dimensionality. For example, the rapidly developing field of molecular magnetism [1] deals mainly with quasi-one-dimensional and quasi-two-dimensional compounds. Although the basic theory of their magnetic properties has been known for a long time [2], it is now necessary to apply it in the various contexts corresponding to these complex molecular architectures.

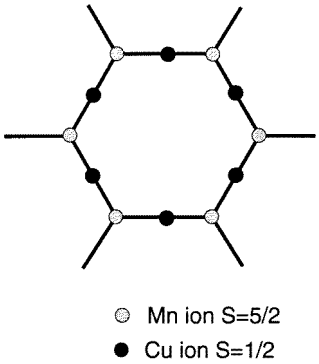

Figure 1. An elementary cell of the hexagonal lattice, with the Cu ions (closed circles) at the mid-points of the links and the Mn ions (open circles) at the vertices.

The compound $(NBu_4)_2Mn_2[Cu(opba)]_3{\cdot}6DMSO{\cdot}H_2O$, first synthesized by Stumpf *et al* [3], exhibits a transition at $T_c = 15$ K towards a ferromagnetically ordered state. The

0953-8984/98/092065+15$19.50

structure of this material can be schematically described as a superposition of negatively charged layers of hexagonal lattices with the Mn^{II} ions (spin 5/2) occupying the vertices and the Cu^{II} ions (spin 1/2) at the mid-points of the links (see figure 1). The tetrabutylammonium cations, NBu_4^+, are located between the layers. Other compounds of the same kind have been synthesized, differing in the nature of the cations between the layers [4]. When these cations are small (Na^+, K^+ and tetramethylammonium), a long-range antiferromagnetic ordering in observed in zero field. An external field of the order of 0.15 kOe is sufficient to overcome the very weak interlayer interactions and to lead to a ferromagnetic-like state. The compounds then behave as metamagnets. When the cations are larger (tetraethylammonium and beyond), a ferromagnetic ordering occurs at a critical temperature T_c. The value of this critical temperature first remains constant and equal to 15 K, then decreases very smoothly as the cation size increases. In other respects, replacing Mn^{II} by a more anisotropic spin carrier such as Co^{II} results in a significant increase of T_c. These results suggest that both interlayer interactions and spin anisotropy are involved in the mechanism of long-range ordering. The role of the spin anisotropy in the magnetic properties of two-dimensional compounds is much less well documented than the three-dimensional effects, and the goal of this paper is to address this problem.

In the layer of $(NBu_4)_2Mn_2[Cu(opba)]_3{\cdot}6DMSO{\cdot}H_2O$, the nearest-neighbour Mn^{II} and Cu^{II} ions interact through an antiferromagnetic coupling. The interlayer interaction in all cases is very small as compared to the intralayer one, so, to a good approximation, the spin system can be considered two dimensional. In a previous paper [5], we showed that such a simple description, in which the spin-5/2 Mn^{II} ions are approximated by classical ones, gives a good account of the magnetic and thermal properties of the paramagnetic phase of the compound. However, since the isotropic O(3) model is critical only at zero temperature [6], we must include a symmetry-breaking mechanism in order to explain the phase transition at $T_c = 15$ K. We attribute this symmetry breaking to the presence of spin anisotropy.

Since no single crystal of the Cu–Mn compound has been obtained so far, a direct measurement of the orientation of the anisotropy is not possible. However, the existence of a spontaneous magnetization below T_c is the signal of an axial anisotropy and of an Ising–like transition. An in-plane anisotropy would have driven the system to become one described by a symmetric XY-model, which, in two dimensions, exhibits a Kosterlitz–Thouless transition with no ordered phase [7].

The aim of this paper is to investigate the effect of a small axial anisotropy in the simple model described above.

For weak anisotropy, the critical properties of the model are dominated by the crossover between the $T = 0$ critical point of the 2D Heisenberg model and the Ising one at T_c. This effect has been widely analysed in the framework of the purely classical Heisenberg model [8–13]. In particular, renormalization group analysis [11] leads to the following result: if λ is the anisotropy parameter ($\lambda = 0$ corresponds to the isotropic case), the Ising critical temperature decreases to zero as

$$T_c(\lambda) \approx \frac{1}{|\ln \lambda|} \qquad \text{for } \lambda \to 0. \tag{1}$$

Furthermore, the zero-field susceptibility satisfies a scaling law

$$\chi(\lambda, T) = \chi(0, T)\Phi(\lambda e^{4\pi/T}) \tag{2}$$

where the function $\Phi(x) \approx |x - x_c|^{-7/4}$ for $x \approx x_c = \lambda e^{4\pi/T_c}$. This equation gives additional information on the Ising critical region. Let us define the width of this region,

δ, by the expression

$$1-\delta \leqslant \frac{T}{T_c} \leqslant 1+\delta \Longrightarrow \chi(\lambda, T) \gg \chi(\lambda = 0, T).$$

From equation (2) we get $\delta \approx 1/|\ln\lambda|$ when $\lambda \to 0$. Therefore in the weak-anisotropy limit we expect the Ising critical region to become very narrow and quite close to $T = 0$. Clearly, this makes experimental investigation difficult.

On the basis of universality, we transpose these renormalization group results to our mixed-spin system. Since we expect the anisotropy to be very small, we need to develop methods specifically designed to handle this crossover effect. In section 2 we present our techniques for high-temperature expansions on the one hand and Monte Carlo simulations on the other hand. In section 3 we analyse our results and, from a comparison with the experimental data, we determine the value of the anisotropy for the Cu–Mn compound. Conclusions are drawn in the last section.

2. The model

We denote by $\boldsymbol{S}_j^{(\mathrm{Mn})}$ the spin-5/2 operator associated with the Mn ion at site j, and by $\boldsymbol{S}_i^{(\mathrm{Cu})}$ the spin-1/2 operator corresponding to the Cu ion at site i in the middle of a link of the honeycomb lattice. The antiferromagnetic interaction is represented by the Heisenberg Hamiltonian

$$\mathcal{H} = J\sum_{\langle i,j\rangle}(\boldsymbol{S}_i^{(\mathrm{Cu})}\cdot\boldsymbol{S}_j^{(\mathrm{Mn})} + \lambda S_i^{z(\mathrm{Cu})}S_j^{z(\mathrm{Mn})}) - \left(\sum_{j=1}^{N_S} g_1\mu_B\boldsymbol{S}_j^{(\mathrm{Mn})} + \sum_{i=1}^{N_L} g_2\mu_B\boldsymbol{S}_i^{(\mathrm{Cu})}\right)\cdot\boldsymbol{H} \qquad (3)$$

where J is positive, λ (>0) is the anisotropy parameter, $\boldsymbol{H}$ is the external magnetic field, $\langle i, j\rangle$ stands for a pair of nearest-neighbour spins, N_S is the number of sites and N_L is the number of links on the honeycomb lattice ($N_L = (3/2)N_S$). The spin-5/2 operator can be approximated by a *classical* spin $S\boldsymbol{s}$ where $\boldsymbol{s}$ is a unit classical vector and $S = \sqrt{(5/2)(5/2+1)}$, whereas the spin-1/2 operators are expressed in terms of the Pauli matrices, $\boldsymbol{S}^{(\mathrm{Cu})} = \frac{1}{2}\boldsymbol{\sigma}$. Since the quantum spin sites are not directly coupled to each other, one can trace out the quantum spin dependence to get a completely classical partition function:

$$Z(T,\boldsymbol{H}) = \int\left(\prod_{i=1}^{N_S}\mathrm{d}\Omega_i\right)\left\{\prod_{\langle ij\rangle} 2\cosh\left|\left|\boldsymbol{W}_{ij} + \frac{1}{2}\beta g_2\mu_B\boldsymbol{H}\right|\right|\right\}\exp\left(\beta g_1\mu_B S\boldsymbol{H}\cdot\sum_{i=1}^{N_S}\boldsymbol{s}_i\right) \qquad (4)$$

where we have defined

$$\boldsymbol{W}_{ij} = -\frac{1}{2}\beta JS(\boldsymbol{s}_i + \boldsymbol{s}_j + \lambda(s_i^z + s_j^z)\hat{\boldsymbol{e}}_z) \qquad (5)$$

and $||\boldsymbol{X}||$ stands for the length of the vector $\boldsymbol{X}$. The indices i and j now label the *classical* spins located at the vertices of the honeycomb lattice.

By choosing the orientation of the magnetic field parallel to the anisotropy axis, or orthogonal to it (along the x-axis), we define $Z_\mu(T, H) \equiv Z(T, H\hat{\boldsymbol{e}}_\mu)$ with $\mu = x$ or z, as follows:

$$Z_\mu(T,H) = \int\left(\prod_{i=1}^{N_S}\mathrm{d}\Omega_i\right)\left\{\prod_{\langle ij\rangle} 2\cosh(K\phi_{\langle ij\rangle}^\mu)\right\}\exp\left(\beta g_1\mu_B SH\sum_{i=1}^{N_S}s_i^\mu\right) \qquad \mu = x \text{ or } z \qquad (6)$$

with $K = \frac{1}{2}\beta JS$ and

$$\phi^{\mu}_{\langle ij\rangle} = \left|\left| \boldsymbol{s}_i + \boldsymbol{s}_j + \lambda(s_i^z + s_j^z)\hat{\boldsymbol{e}}_z - \frac{g_2\mu_B}{JS} H\hat{\boldsymbol{e}}_\mu \right|\right|.$$

We shall be interested in the standard observables: the specific heat

$$C_V = k_B\beta^2 \frac{\partial^2}{\partial\beta^2} \ln Z(T, 0)$$

and the susceptibility along the different directions

$$\chi_\mu = \frac{k_B T}{V} \frac{\partial^2}{\partial H^2} \ln Z_\mu \Big|_{H=0}$$

and also the total susceptibility

$$\chi = \frac{1}{3}\chi_z + \frac{2}{3}\chi_x$$

which is measured experimentally.

3. The method of analysis

3.1. The high-temperature expansion

We have performed the expansion of $\ln Z_\mu$ in power series in K up to the 19th order and to the second order in H for computing the magnetic susceptibility. Then we analysed the series for decreasing values of the anisotropy parameter. The complexity of the nearest-neighbour interaction (equation (6)) prevents one from using the standard techniques [8, 14, 15].

The diagrammatic expansion is generated by replacing in equation (6) each $\cosh(K\phi^{\mu}_{\langle ij\rangle})$ term by $1 + \Psi^{\mu}_{\langle ij\rangle}$ where the function $\Psi^{\mu}_{\langle ij\rangle}$ results from the expansion of the hyperbolic cosine in a power series in K to the given maximal order and of H to second order. To each function $\Psi^{\mu}_{\langle ij\rangle}$ appearing in the product over the nearest-neighbour pairs in equation (6) is associated one link of a graph G. Hence, only single-line graphs will appear; moreover, since the contribution of each link starts as K^2, a graph with n links will contribute at least to the order K^{2n}. We have performed this expansion on our hexagonal lattice up to nine-line diagrams, leading to a maximal order† of K^{19}.

The powerful star graph expansion technique [15] cannot be used here since, due to the presence of the anisotropy term, the partition function of articulated graphs does not factorize. Our procedure is based on the standard connected graph expansion [15] for the normalized partition function $\widetilde{Z}_\mu = Z_\mu(T, H)/Z_\mu(T, H)|_{J=0}$, namely

$$\ln \widetilde{Z}_\mu(T, H) = \sum_{\{G\}} C(G)\omega(G)$$

where $\{G\}$ is the set of all connected graphs to a given order, $C(G)$ are the embedding constants of the graph G, and $\omega(G)$ is its weight. The weights $\omega(G)$ are constructed through the recursive technique:

$$\ln \widetilde{Z}_\mu(G) = \sum_{\{g\}} \omega(g)$$

where $\{g\}$ is the set of all subgraphs of G.

† Odd terms appears through the magnetic field dependence of the exponential kernel of equation (6).

The construction of the graphs and the counting of their embedding numbers have been automated in a Maple V program. We have developed a recursive algorithm based on the standard technique of reference [16], which is sufficiently efficient for the small number of graphs involved here†.

The main difficulty of the method resides in the computation of $\ln \widetilde{Z}_\mu(G)$, which is given by

$$\ln \widetilde{Z}_\mu(G) = \int \left(\prod_{i \in G} \mathrm{d}\Omega_i \right) \left(\prod_{\ell \in G} \Psi_\ell^\mu \right) \exp\left(\beta g_1 \mu_B S H \sum_{i \in G} s_i^\mu \right) \tag{7}$$

where $\{\ell\}$ and $\{i\}$ are respectively the set of links and the set of vertices belonging to the graph G. We proceed as follows.

(a) By using the spherical harmonic basis and the reduction formula [15, 17, 18], each function $\Psi^\mu_{\langle ij \rangle}$ can be expressed as

$$\Psi^\mu_{\langle ij \rangle} = \sum_{l_1 m_1 l_2 m_2} \Lambda^{l_2 m_2}_{l_1 m_1} Y_{l_1 m_1}(\Omega_i) Y_{l_2 m_2}(\Omega_j)$$

where $\Lambda^{l_2 m_2}_{l_1 m_1}$ is a matrix built up recursively of elements which are power series in K and in H.

(b) The exponential term in equation (7) is expanded to second order in H, and the spin dependence expressed in terms of the spherical harmonics.

(c) The integral is then computed, contracting the products of spherical harmonics by means of the reduction formula through the Clebsch–Gordan algebra [18], and then integrating over the residual angular variables.

All of these steps have been performed algebraically by means of a Maple V program. We obtain a series in powers of K of which the coefficients are polynomials in λ and in g_1 and g_2. As an illustration of our results, we give in table 1 the coefficients‡ of the development of χ_z to the zeroth and first order in λ.

We have verified that the weight ω of each articulated graph is proportional to λ. Thus, for $\lambda = 0$ we recover the property of the star graph expansion of the isotropic model. We check that, in this case, all of our series coincide algebraically with the ones obtained in reference [5] by completely different methods.

The Padé extrapolation technique [19] is used to analyse the series of the various observables, normalized to their isotropic counterpart in order to enhance the effect of the anisotropy. More explicitly, we predict that at $T_C(\lambda)$ the heat capacity diverges logarithmically and the axial susceptibility diverges with the Ising exponent 7/4.

For our system [5], the renormalization group result of equation (2) becomes for the axial susceptibility χ_z

$$\frac{\chi_z(\lambda, K)}{\chi_z(0, K)} = \Phi(\lambda \mathrm{e}^{(2\pi/\sqrt{3})K}) \qquad \text{with } K = \frac{1}{2}\beta J S \tag{8}$$

where the function $\Phi(x) \approx |x - x_c|^{-7/4}$ for $x \approx x_c = \lambda \mathrm{e}^{(2\pi/\sqrt{3})K_c}$. For small λ, the singularity is located at large values of K, far away from the perturbative region. We analysed the function $(\chi_z(\lambda, K)/\chi_z(0, K))^{4/7}$ in terms of the variable $v = 1 - \mathrm{e}^{-\alpha K}$, small at high temperature but bounded for large K. According to equation (8), this function is expected to have a simple pole at $v = v_c(\alpha)$ which is found as a zero of the denominator

† There are only 45 independent connected graphs with 9 undirected single links on the honeycomb lattice.

‡ The complete set of coefficients for all of the series can be obtained on request from the authors; e-mail: meyers@bortibm1.in2p3.fr.

Table 1. A subset of the coefficients of the high-temperature series for the axial susceptibility χ_z in powers of $K = \frac{1}{2}\beta JS$ up to the 17th order. The coefficient of K^n is a polynomial of degree n in the anisotropy parameter λ. For each coefficient we only give the constant term and the term linear in λ (the columns headed λ^0 and λ^1respectively). The top half of the table contains the even-power coefficients; for each power of λ the fraction of the first sub-column must be multiplied by $S^2g_1^2$ and added to the second multiplied by g_2^2. For instance, the coefficient of K^2 is $\frac{2}{9}S^2g_1^2 + \frac{2}{9}g_2^2 + \lambda(\frac{28}{45}S^2g_1^2 + \frac{2}{3}g_2^2) + \mathrm{O}(\lambda^2)$. The bottom half of the table contains the odd-power coefficients; the fraction in each column must be multiplied by Sg_1g_2.

	λ^0		λ^1	
	$S^2g_1^2$	g_2^2	$S^2g_1^2$	g_2^2
K^0	$\frac{2}{9}$	$\frac{1}{4}$	0	0
K^2	$\frac{2}{9}$	$\frac{2}{9}$	$\frac{28}{45}$	$\frac{2}{3}$
K^4	0	$-\frac{1}{15}$	$\frac{32}{81}$	$\frac{6}{25}$
K^6	$\frac{2}{225}$	$\frac{533}{8505}$	$\frac{1532}{30\,375}$	$\frac{5282}{42\,525}$
K^8	$-\frac{4}{2835}$	$-\frac{5683}{127\,575}$	$\frac{512}{14\,175}$	$-\frac{1754}{25\,515}$
K^{10}	$\frac{524}{893\,025}$	$\frac{19\,912}{601\,425}$	$-\frac{128\,824}{9568\,125}$	$\frac{219\,628}{2525\,985}$
K^{12}	$-\frac{69\,464}{35\,083\,125}$	$-\frac{51\,038\,503}{1915\,538\,625}$	$\frac{117\,344}{526\,246\,875}$	$-\frac{14\,083\,390\,696}{143\,665\,396\,875}$
K^{14}	$\frac{4539\,614}{1149\,323\,175}$	$\frac{6380\,434}{273\,648\,375}$	$\frac{5687\,869\,652}{430\,996\,190\,625}$	$\frac{20\,243\,410\,804}{184\,712\,653\,125}$
K^{16}	$-\frac{408\,296\,024}{86\,199\,238\,125}$	$-\frac{87\,518\,482\,699}{4396\,161\,144\,375}$	$-\frac{62\,768\,262\,944}{4114\,054\,546\,875}$	$-\frac{3168\,011\,262\,218}{29\,973\,825\,984\,375}$

	λ^0	λ^1
	Sg_1g_2	Sg_1g_2
K^1	$-\frac{2}{3}$	$-\frac{2}{3}$
K^3	$-\frac{2}{27}$	$-\frac{166}{135}$
K^5	$-\frac{8}{405}$	$-\frac{152}{675}$
K^7	$\frac{2}{8505}$	$-\frac{69\,758}{637\,875}$
K^9	$-\frac{4}{4725}$	$\frac{44\,524}{1913\,625}$
K^{11}	$\frac{7108}{49\,116\,375}$	$-\frac{316\,875\,236}{11\,051\,184\,375}$
K^{13}	$\frac{45\,214\,696}{5746\,615\,875}$	$\frac{11\,621\,348\,744}{143\,665\,396\,875}$
K^{15}	$-\frac{2434\,334\,054}{86\,199\,238\,125}$	$-\frac{130\,568\,299\,906}{587\,722\,078\,125}$
K^{17}	$\frac{875\,743\,046\,944}{13\,987\,785\,459\,375}$	$\frac{419\,699\,964\,912\,544}{887\,686\,384\,921\,875}$

of the Padé approximants in the variable v. The parameter α is chosen by minimizing the dispersion of the poles of the central approximants. The residual dispersion gives an estimate of the error in the critical temperature obtained by this method. For very low values of λ, this method becomes inaccurate, giving large error bars.

The series for the heat capacity and for the in-plane susceptibility have been summed along analogous lines.

For $\lambda \lesssim 10^{-2}$ an extension of the series to higher orders is needed to reliably determine the critical temperature. However, in this regime of very weak anisotropy, once the critical temperature is known by another method—Monte Carlo simulation for instance—the series becomes a useful analytic representation of the observables. It will be used to determine the physical parameters from a comparison with the experimental data.

The results of this analysis will be presented and discussed in the next section together with the Monte Carlo results.

3.2. The Monte Carlo simulation

We performed a Monte Carlo simulation in order to verify the results of the high-temperature expansion, and to investigate the regime of very small anisotropy where the perturbative technique fails. The simulation is based on the effective classical model

$$-\beta\mathcal{H}_{\text{eff}} = \sum_{\langle ij\rangle} \ln(2\cosh||\boldsymbol{W}_{ij}||) \tag{9}$$

where $\boldsymbol{W}_{ij}$ is defined in equation (5). The various observables can be expressed as ensemble averages with respect to the Boltzmann weight $\mathrm{e}^{-\beta\mathcal{H}_{\text{eff}}}/Z(T,0)$. Their expression is a simple generalization of the definition of equations (6) and (8) of reference [5] in which W_{ij} is replaced by the new definition of equation (5).

Our goal is to explore the weak-anisotropy regime where the effect of crossover between the 2D Heisenberg and Ising fixed points is important. As the anisotropy gets smaller, most of the low-temperature region is dominated by the 2D Heisenberg regime in which the correlation length remains large due to the essential singularity at $T = 0$. Therefore, the usual limitations of the Monte Carlo procedure—critical slowing down and the finite-size effects—constrain the simulation of these systems rather severely.

In order to overcome the first problem we used a global algorithm. We have adapted the Wolf algorithm [20] to the case of an anisotropic interaction. The 'Ising' orientation of the spins, used to construct the Wolf cluster and which is randomly chosen in the standard algorithm, is imposed here by the anisotropy. In our procedure, a Monte Carlo update proceeds in three steps:

(i) construct a first cluster with respect to the z- (anisotropy) axis and flip the corresponding spin components;

(ii) construct another cluster relative to a randomly chosen direction in the x–y plane and flip the corresponding spin components.

After these two steps, a given spin remains on the cone defined by its initial orientation and the z-axis. Therefore we proceed to another step:

(iii) change the actual orientation of each spin of the lattice according to a standard Metropolis algorithm. This operation is repeated twice.

In a typical run we perform 5000 MC steps of thermalization followed by 10^5 measurements divided into 100 bins of 1000 MC steps for the error analysis. We used the standard IBM congruent random-number generator drand48. Down to moderately weak anisotropy

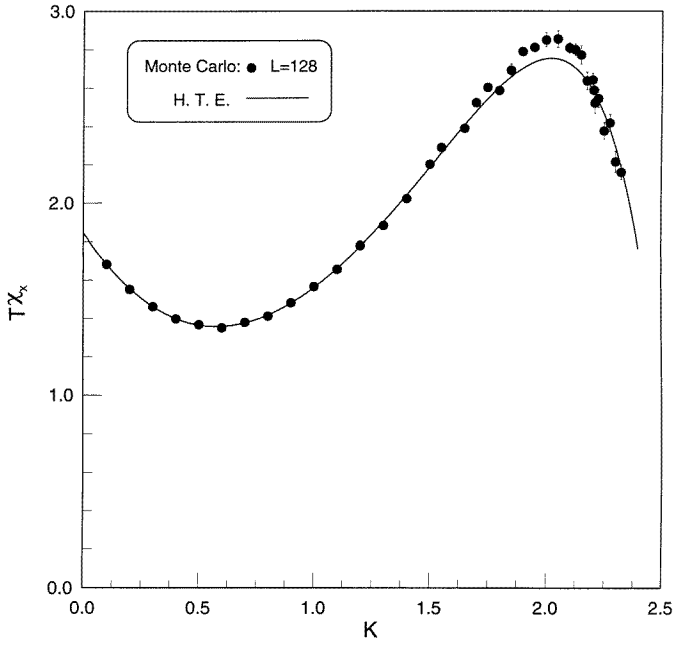

(a)

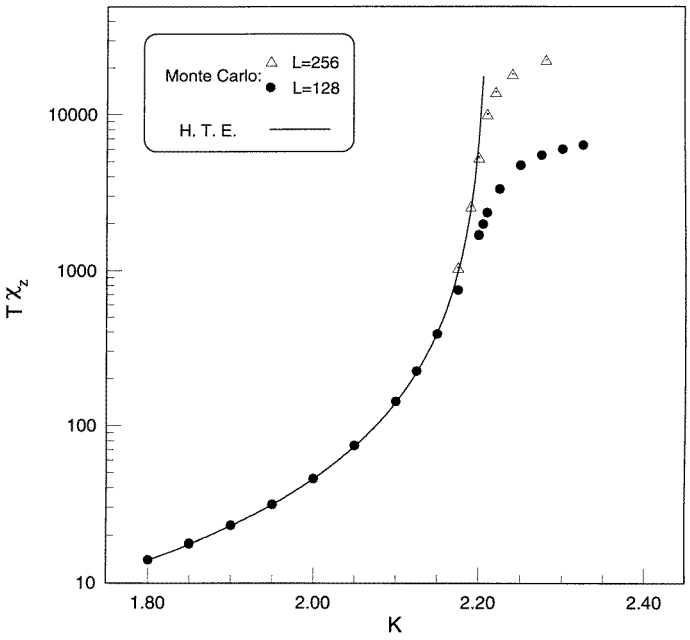

(b)

Figure 2. The susceptibility multiplied by the temperature, as a function of the reduced coupling $K = \frac{1}{2}\beta JS$ for an anisotropy $\lambda = 0.1$. The data points come from the Monte Carlo simulation; the solid line corresponds to the Padé approximant of the high-temperature expansion (HTE). (a) The in-plane susceptibility. (b) The axial susceptibility. The closed circles correspond to a lattice size $L = 128$ and the triangles to $L = 256$.

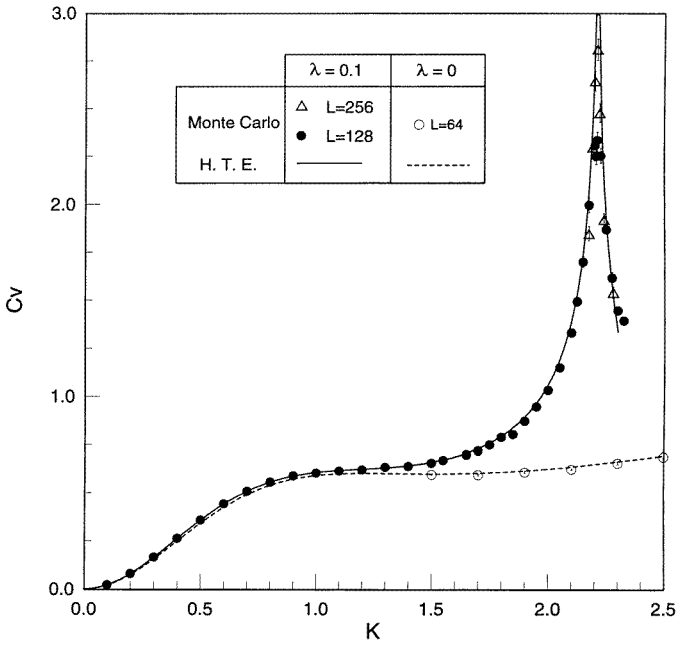

Figure 3. The specific heat as a function of K. For an anisotropy parameter $\lambda = 0.1$: the Monte Carlo data are represented by the closed circles for a lattice size $L = 128$ and by open triangles for $L = 256$. The solid line corresponds to the high-temperature expansion (Padé approximant). For the isotropic model ($\lambda = 0$): the open circles correspond to the Monte Carlo simulation ($L = 64$) and the dashed line to the series result.

($\lambda \gtrsim 10^{-2}$) the decorrelation time remains small—5 to 25 Monte Carlo steps, depending on the temperature. However, when λ decreases, the domain of temperature to be investigated gets closer to zero and the Metropolis part of our Monte Carlo procedures induces larger decorrelation times. Furthermore, in this region, the correlation length remains large even outside the Ising critical region, inducing non-negligible finite-size effects. Therefore, we limited our analysis to $\lambda = 0.001$ and to a maximum lattice size of $L = 256$ for which we checked that all of these effects remain negligible†. With this procedure we recover the results of the zero-anisotropy case [5], and of the strong-anisotropy (classical Ising) limit with a good accuracy.

4. Results

4.1. The critical temperature

To validate our methods we compare the results obtained by the two procedures. We present in figure 2 the zero-field susceptibility, orthogonal to the anisotropy axis (χ_x) and parallel to it (χ_z) for the high-temperature series and the Monte Carlo data as a function of K and for a moderately small value of the anisotropy parameter $\lambda = 0.1$. The agreement between these two sets of results is very good. These curves clearly show the divergent behaviour of the axial susceptibility, which will be used to determine the critical temperature in the

† In this case, close to the critical temperature, the decorrelation time is of order 70 MC steps, and thus much smaller than the width of the bins used in the data analysis.

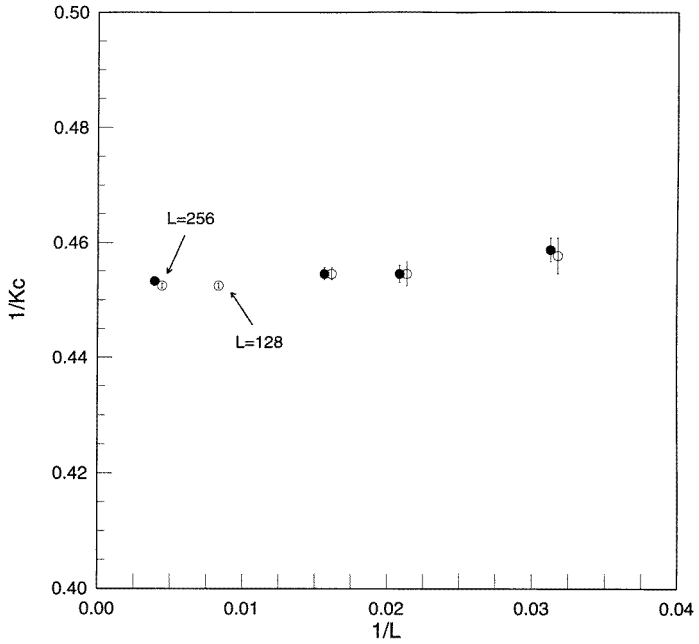

(a)

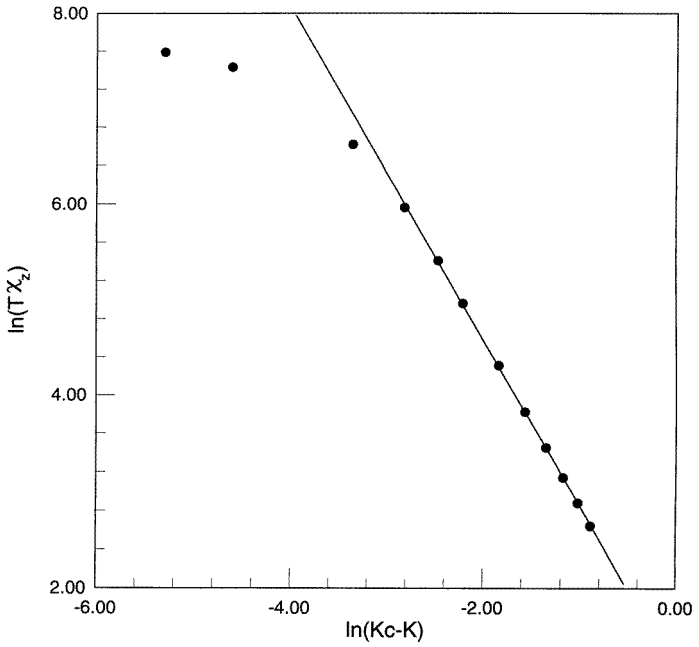

(b)

Figure 4. Analysis of the Ising critical regime. (a) The finite-size critical temperature as a function of the lattice size L: from the maximum of the specific heat (triangles); from the inflexion point of the axial susceptibility (circles). (b) the axial susceptibility as a function of $|K_c - K|$ on a log–log scale. The slope of the fitted straight line is 1.74(2), in good agreement with the expected exact Ising value, $\gamma = 1.75$.

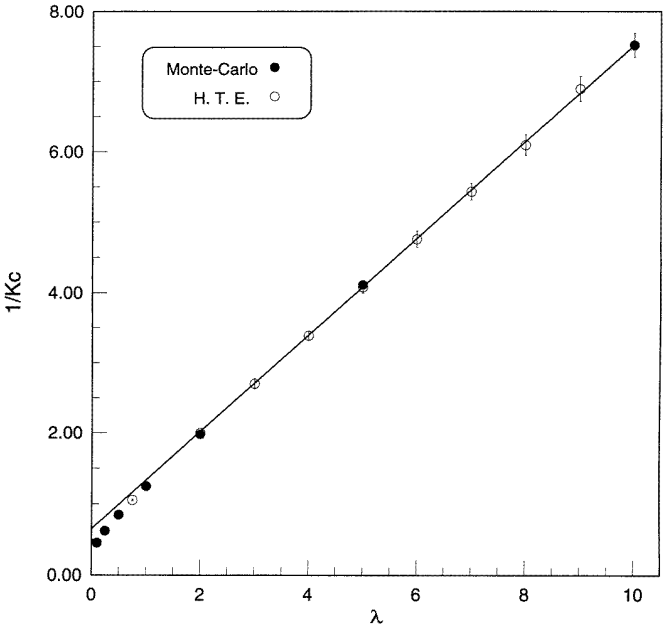

(a)

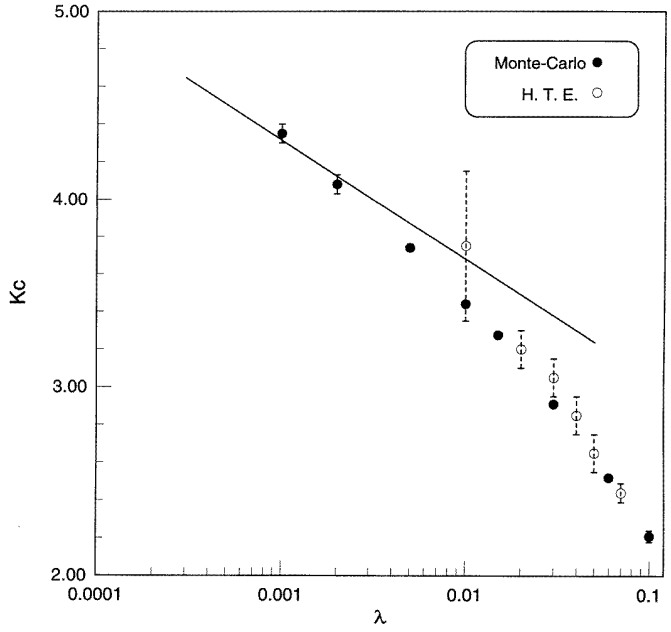

(b)

Figure 5. The variation of the critical temperature with λ. The series results are represented by open circles and the Monte Carlo simulation by closed circles. (a) The strong-anisotropy regime: we plot the inverse of the reduced critical coupling $K_c^{-1} = 2k_B T_C/JS$ as a function of the anisotropy parameter. The slope of the linear behaviour expected at large λ corresponds to $K_{c\ \mathrm{Ising}} \simeq 1.46(1)$. (b) The weak-anisotropy regime: the reduced critical coupling K_c as a function of λ on a logarithmic scale. The solid line corresponds to the renormalization group behaviour, $K_c = -(\sqrt{3}/2\pi)\ln\lambda + \text{constant}$. The value of the constant is 2.41(2).

Monte Carlo simulation. Figure 3 displays the specific heat as a function of K for the same anisotropy. Besides the good agreement between the two methods, we observe the clear critical signal at $K_c \simeq 2.21$ which emerges from the comparison with the result for the isotropic model.

The critical temperature is obtained from the Monte Carlo data by localizing the peak in the specific heat and the inflexion point of the susceptibility as a function of the temperature. In order to estimate the precision of such a determination, we performed a complete finite-size scaling analysis of the data at $\lambda = 0.1$ to obtain the critical temperature and the susceptibility exponent. The results are presented in figure 4 where we plotted $T_c(L)$, measured from the two signals, for several lattice sizes (figure 4(a)), and (in figure 4(b)) $\ln \chi$ as a function of $\ln|K_c - K|$. Figure 4(a) shows a small variation of the finite-system critical signal, which allows us to estimate the bulk critical temperature T_c from lattices of size not exceeding $L = 128$. With this estimate, we determine the exponent γ of the susceptibility from figure 4(b). The result $\gamma = 1.74(2)$ is in very good agreement with the expected exact Ising value $\gamma = 1.75$. This is a self-consistent indication of the reliability of the critical temperature measurement. Furthermore, we checked that the Monte Carlo result falls within the error bar obtained from the high-temperature series analysis.

With this method, we determined the critical coupling

$$K_c = \frac{1}{2}\frac{JS}{k_B T_c}$$

as a function of the anisotropy parameter on lattices of size $L \leqslant 256$ down to $\lambda = 0.001$. The results of the two analyses—Monte Carlo and high-temperature expansion—are displayed in figure 5. Figure 5(a) shows the general trend of the variations of $K_c^{-1} \propto T_c$ as a function of λ, with a decrease to zero for $\lambda \to 0$, and a linear variation at large λ. In fact, for $\lambda \to \infty$, the model coincides with a classical Ising model with coupling $K_{\text{Ising}} = \lambda K$ so, in this limit, $K_c^{-1}(\lambda) \simeq \lambda K_{c\ \text{Ising}}^{-1}$. From the high-temperature expansion, we get the estimate $K_{c\ \text{Ising}} \simeq 1.46(1)$. The variations for small λ are presented in figure 5(b) where we plotted K_c versus $\ln \lambda$. It appears that the behaviour predicted on the basis of the renormalization group (equation (1)) is obtained for very small anisotropy. In fact, from figure 5(b) we obtain

$$K_c = \frac{\sqrt{3}}{2\pi}|\ln \lambda| + 2.41 \qquad \lambda \lesssim 0.001. \tag{10}$$

Therefore, by extrapolating this behaviour down to $\lambda \to 0$, we are able to predict the critical temperature for very small anisotropy.

4.2. Comparison with the experimental results.

In order to compare with the experimental results, we proceed in two steps.

(i) We get an estimation of the anisotropy parameter from the value of J previously determined in the analysis of the paramagnetic phase [5] and from the experimental critical temperature $T_c = 15$ K. We obtain $K_c \simeq 4.6$ which corresponds to $\lambda \simeq 0.0004$, according to figure 5(b).

(ii) We perform an adjustment of J, g_1 and g_2 at fixed λ by fitting the experimental data with a selected Padé approximant. Small variations around the fixed λ-value do not significantly change the fit.

The results are presented in figure 6—for the whole range of temperature in figure 6(a) and for the critical region only in figure 6(b). An excellent agreement with the experimental

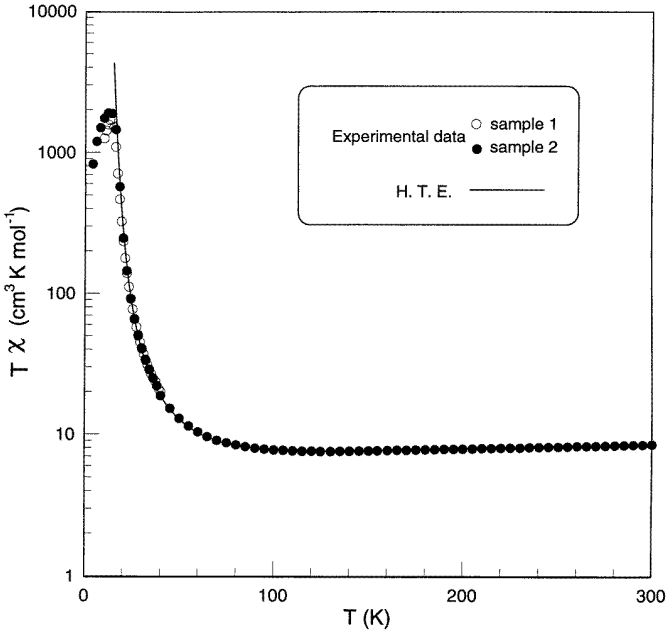

(a)

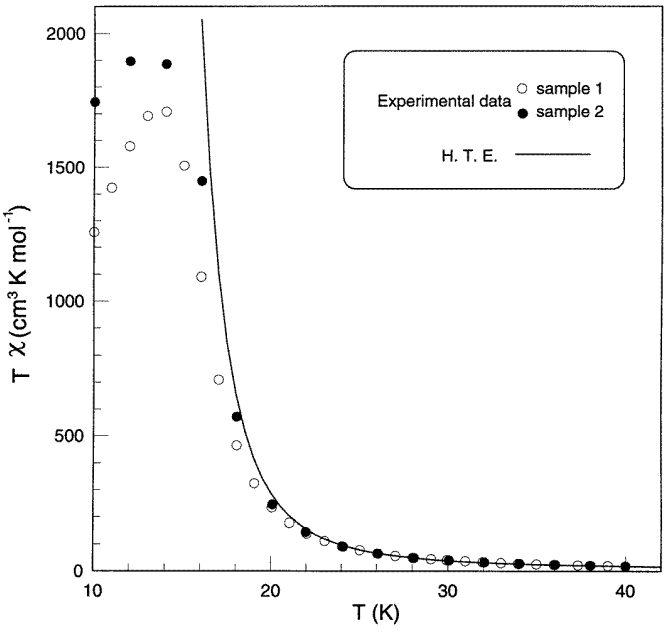

(b)

Figure 6. Fits of the experimental data (closed circles for sample 1, open circles for sample 2) for the total magnetic susceptibility. The solid line corresponds to a Padé approximant of the high-temperature series with the following parameters: $J = 45.5$ K, $g_1 = 2.0$, $g_2 = 2.14$, $\lambda = 0.0005$; (a) for the whole temperature range; (b) for the critical region. The difference between the results for the two samples gives an estimation of the experimental errors in the critical region.

data is obtained with the following set of parameters:

$$J = 45.5 \text{ K} \qquad g_1 = 2.0 \qquad g_2 = 2.11 \qquad \lambda \simeq 0.0005.$$

The exponential variation of λ with respect to T_c (equation (10)) induces a rather large error bar in the determination of λ; in fact, an error of one degree Kelvin in T_c induces a variation of λ by a factor of 3. However, the magnetic susceptibility is rather insensitive to these variations, which only affect the Ising critical region over such a narrow range of temperature that it is not visible experimentally. Moreover, the high-temperature ($T \geqslant 50$ K) behaviour is left completely unchanged by such a small perturbation, thus preserving the good agreement with the isotropic model observed in reference [5].

5. Conclusions

We have determined the spin anisotropy which is present in the Cu–Mn magnetic compound [3] and which is responsible for a ferromagnetic transition at 15 K. Two methods—high-temperature expansion and Monte Carlo simulation—are used in a complementary way in order to extract reliable results for the strong-crossover regime where the effect lies. Assuming universality and extending the renormalization group results to our situation, we obtain a very small value for the anisotropy parameter.

The strong behaviour $T_c(\lambda) \approx 1/|\ln \lambda|$ is responsible for the fact that a very weak perturbation ($\lambda \simeq 10^{-4}$) produces a sizable effect ($T_c \simeq 15$ K). For these quasi-two-dimensional molecular compounds, involving high-spin magnetic ions, it is inconceivable that, at such a low level of magnitude, anisotropy is absent. Therefore we should always expect a ferromagnetic transition at an appreciable critical temperature in these systems.

In this work, we only considered the exchange anisotropy as a source of the O(3) symmetry breaking. Alternatively, on-site anisotropy could be present, but in the limit of weak anisotropy under consideration here, on the grounds of universality, we expect the results to be unchanged. As regards the interlayer interactions which have been neglected in our approach, it is known [12] that if the ratio of the interlayer coupling to the intralayer coupling, $\sigma = J_\perp/J_\parallel$, is small, the transition temperature induced by these three-dimensional effects behaves like $T_c \approx 1/\ln|\sigma|$. Therefore, even a very small interplane coupling may significantly contribute to the measured critical temperature, in competition with the anisotropy effect. We have seen that increasing the interlayer distance beyond a certain limit results in a smooth decrease of T_c. Taking into account the interlayer coupling would require us to introduce an additional effect of crossover between the three-dimensional model with spatial anisotropy and the two-dimensional one with exchange anisotropy [12]. As a consequence, the contribution of the spin anisotropy to the critical temperature would be overestimated and our result for the anisotropy parameter would turn out to be an upper bound.

Acknowledgments

We wish to thank S V Meshkov for his contribution to the Monte Carlo part of this work and J Leandri for helpful discussions.

References

[1] Kahn O 1993 *Molecular Magnetism* (New York: VCH)
[2] Heisenberg W 1928 *Z. Phys.* **49** 619

[3] Stumpf H O, Yu Pei, Kahn O, Sletten J and Renard J P 1993 *J. Am. Chem. Soc.* **115** 6738
[4] Cador O, Price D, Larionova J, Mathonière C, Kahn O and Yakhmi J V 1997 *J. Mater. Chem.* **7** 1263
[5] Leandri J, Leroyer Y, Meshkov S V, Meurdesoif Y, Kahn O, Mombelli B and Price D 1996 *J. Phys. C: Solid State Phys.* **8** L271
[6] Mermin N D and Wagner H 1966 *Phys. Rev. Lett.* **17** 1133
[7] Kosterlitz J M and Thouless D J 1973 *J. Phys. C: Solid State Phys.* **6** 1181
[8] Jasnow D and Wortis M 1968 *Phys. Rev.* **176** 739
[9] Pfeuty P, Jasnow D and Fisher M E 1974 *Phys. Rev.* B **10** 2088
[10] Binder K and Landau D P 1976 *Phys. Rev.* B **13** 1140
[11] Pelcovits R A and Nelson D R 1976 *Phys. Lett.* **57A** 23
Nelson D R and Pelcovits R A 1977 *Phys. Rev.* B **16** 2191
[12] Hikami S and Tsuneto T 1979 *Prog. Theor. Phys.* **63** 387
[13] Cuccoli A, Tognetti V and Vaia R 1995 *Phys. Rev.* B **52** 10 221
[14] Rushbrooke G S, Baker G A and Wood P J 1974 *Phase Transitions and Critical Phenomena* vol 3, ed C Domb and M S Green (New York: Academic) p 246
[15] McKenzie S 1980 *Phase Transitions (NATO ASI Series B, vol 72)* (New York: Plenum) p 271
[16] Martin J L 1974 *Phase Transitions and Critical Phenomena* vol 3, ed C Domb and M S Green (London: Academic) p 97
[17] Joyce G S 1966 *Phys. Rev.* **155** 478
[18] Rotenberg M, Bivins R, Metropolis N and Wooten J K Jr 1959 *The 3j and 6j Symbols* (London: Crosby, Lockwood & Son)
[19] Bender C M and Orszag S A 1978 *Advanced Mathematical Methods for Scientists and Engineers* (New York: McGraw-Hill)
[20] Wolf U 1989 *Phys. Rev. Lett.* **62** 361
Wolf U 1990 *Nucl. Phys.* B **344** 581